Orbital graph convolutional neural network for material property prediction

Mohammadreza Karamad,[1,2,*] Rishikesh Magar,[2,*] Yuting Shi,[2] Samira Siahrostami,[3]
Ian D. Gates,[1] and Amir Barati Farimani[2,†]

[1]*Department of Chemical and Petroleum Engineering, University of Calgary, 2500 University Drive NW Calgary, Alberta T2N 1N4, Canada*
[2]*Department of Mechanical Engineering, Chemical Engineering, and Biomedical Engineering, Carnegie Mellon University, Pittsburgh, Pennsylvania 15213, USA*
[3]*Department of Chemistry, University of Calgary, 2500 University Drive NW, Calgary, Alberta T2N 1N4, Canada*

(Received 12 February 2020; accepted 11 August 2020; published 8 September 2020)

Material representations that are compatible with machine learning models play a key role in developing models that exhibit high accuracy for property prediction. Atomic orbital interactions are one of the important factors that govern the properties of crystalline materials from which the local chemical environments of atoms is inferred. Therefore, to develop robust machine learning models for material properties prediction, it is imperative to include features representing such chemical attributes. Here, we propose the orbital graph convolutional neural network (OGCNN), a crystal graph convolutional neural network framework that includes atomic orbital interaction features that learns material properties in a robust way. In addition, we embedded an encoder-decoder network into the OGCNN enabling it to learn important features among basic atomic (elemental features), orbital-orbital interactions, and topological features. We examined the performance of this model on a broad range of crystalline materials data to predict different properties. We benchmarked the performance of the OGCNN model with that of: (1) the crystal graph convolutional neural network, (2) other state-of-the-art descriptors for material representations including many-body tensor representation and the smooth overlap of atomic positions, and (3) other conventional regression machine learning algorithms where different crystal featurization methods have been used. We find that the OGCNN significantly outperforms them. The OGCNN model with high predictive accuracy can be used to discover new materials among the immense phase and compound spaces of materials.

DOI: 10.1103/PhysRevMaterials.4.093801

I. INTRODUCTION

Owing to the methodological improvements in *ab initio* calculations, such as density functional theory (DFT) as well as increasing computing power, it has now become possible to perform high-throughput computational calculations to search for new materials with specific properties of interest [1–5]. However, *ab initio* high-throughput computational methods are hampered by expensive calculations necessitating development of alternative methods to predict material properties. Machine learning (ML) techniques, on the other hand, have proven to provide a fast and accurate way to predict desired properties enabling facile discovery of new materials at a fraction of the computational cost and in a shorter timescale. ML algorithms build a functional map between the input data representing the material and the output data being the properties of interest. These models have been used to predict a wide range of properties for different classes of material [6–16]. One of the important challenges to develop a ML-based approach for predicting material properties is material representation, i.e., encoding material information, including features (also often called the descriptors), geometrical, and topological information [17].The features need to be unique in representing material, they should be computed at low computational cost or preferably be readily accessible from available databases. Most importantly, they should reflect the chemical information related to the targeted properties. This requires encoding the information about electronic structure, chemistry as well as the topology of the material. In addition, feature vector representation needs to be compatible with the ML model. To this end, developing features that possess the aforementioned properties has proven to be challenging [6].

Roughly speaking, for a given crystalline material, the information related to its physical and chemical properties arise from the position of charges and nuclei, the topology of the crystal, basic properties of its constituent elements, and interatomic interactions. Furthermore, key information about the local chemical environments of atoms forms the fundamental basis to determine the properties of the crystals. Therefore, the accuracy of a ML model to predict material properties is mostly controlled by the ability of its descriptors to accurately encode the local chemical environments of atoms [17]. Different methods to represent the local chemical environments of atoms have been developed. Examples include using atom-distribution-based symmetry functions [18,19], smooth overlap of atomic positions [17], many-body tensor representation [20], band structures and density of states descriptors [21], and the Coulomb matrix

*These authors contributed equally to this work.
†Corresponding author: barati@cmu.edu

(CM) representation [22]. In many of these methods, structural or elemental information or both have been used as features for representation. The elemental features are either intrinsic quantities, such as the atomic number and ionization energy or heuristic quantities, such as the electronegativity and ionic radius [21,23,24]. Structural representations, on the other hand, encode local chemical environments by capturing the geometry and interaction between atoms [22,25]. Another interesting attempt for crystal representation uses electronic structure attributes [9,21]. This is important because the electronic structure is one of the key parameters in defining material properties. The electron configurations and orbital-orbital interactions are important electronic structure attributes which should be included as representations for ML predictions. Including such information, however, often requires performing DFT calculations to generate descriptors which, consequently, increases computational costs [21]. Different efforts have been made to represent material by considering electronic structure attributes without performing DFT calculations [23,26]. Ward *et al.* used an extensive set of features, including basic atomic and electronic structure features to develop a ML model for predicting different crystalline properties [9,23]. They used the average fraction of electrons from the s, p, d, and f valence shells of all present elements to quantitatively represent atomic electronic states as electronic structure attributes. Clearly, such representations do not explicitly include orbital interactions among constituent elements of the crystals. In another work, Pham *et al.* developed a novel two-dimensional descriptor called the orbital field matrix (OFM) that encodes orbital interactions according to electron configurations of the central atom and neighbor atoms surrounding the central atom [26]. In the OFM, a simple description of the interaction of valence electrons of a central atom with its neighbor atoms represents orbital-orbital interactions. The OFM model showed promise to predict different material properties including formation energy and atomization energy by using conventional ML algorithms, such as kernel ridge regression, decision tree regression, and random forest regression. Despite its promise, the OFM model does not include any elemental atomic features, kernelized distance features, or graph representation of the crystals. In addition, the OFM model did not use the state-of-the-art deep learning techniques.

Deep learning has been widely used in materials science research and molecular property prediction [27–31]. In particular, convolutional neural networks (CNNs) have been used for material properties prediction because of their special ability to extract features from the data [32]. In a recent study by Cao *et al.*, Magpie and OFM descriptors were used in conjunction with the CNN to predict material properties [33]. The reported prediction accuracy for training formation energies of a dataset of alloys is significantly higher than using either of the descriptors. However, Cao *et al.*, did not use graph representation for crystalline systems, feature representation, and dimensionality reduction. Recently, Xie and Grossman, developed a crystal graph convolutional neural network (CGCNN) framework to represent periodic crystalline systems for predicting material properties [34]. In the CGCNN, a graph representation was used to describe the structure of the crystals. In addition, the crystal information was encoded using basic atomic features, such as electron affinity and group number. To encode the neighboring atoms' geometrical effects, the interatomic interactions using their atomic distances were considered. The CGCNN model has many powerful characteristics, such as inclusion of kernelized distance features, features encoding via dimensionality reduction, and convolution of the atom features with its neighbors. Although the CGCNN model demonstrates the ability to predict a variety of properties with high accuracy, it does not consider the attributes that contain orbital-orbital interaction features. In this contribution, we develop a graph convolutional neural network that incorporates the atomic orbital interactions. This new model is referred to as the orbital graph convolutional neural network (OGCNN). The inclusion of orbital-orbital interactions to encode the local chemical environments of atoms along with embedding of an encoder-decoder network enabled the OGCNN to achieve higher accuracy compared to the CGCNN. To show the robustness of the OGCNN model, we benchmarked it against the CGCNN, other state-of-the-art descriptors for material representations including the many-body tensor representation (MBTR) and the smooth overlap of atomic positions (SOAP), and a variety of conventional ML models with different crystalline material representations.

II. MODEL ARCHITECTURE

To include atomic orbital interactions, we employed the representation of crystal systems named OFMs where the atomic orbital interactions are counted based on the distribution of valence shell electrons [26,35]. In the OFM model, the electron configuration of each atom is converted into a one-dimensional (1D) binary vector, and the local structure surrounding an atom is encoded into a matrix that is the sum of the weighted vector representation of all neighboring atoms [Eq. (1)].

To better explain the OFM, let us take an example, a FeTi alloy with body-centered-cubic crystal structure as shown in Fig. 1. The center Fe atom, denoted as c, is surrounded by 14

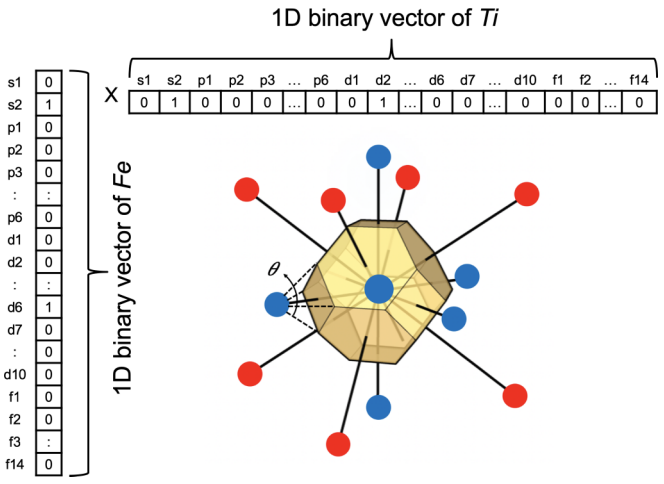

FIG. 1. The OFM representation for the FeTi alloy. Blue and red atoms are Fe and Ti, respectively. The inset shows the Voronoi polyhedron for the center Fe atom forming a truncated octahedron. The 1D binary vectors for the Fe and Ti atoms are shown as well.

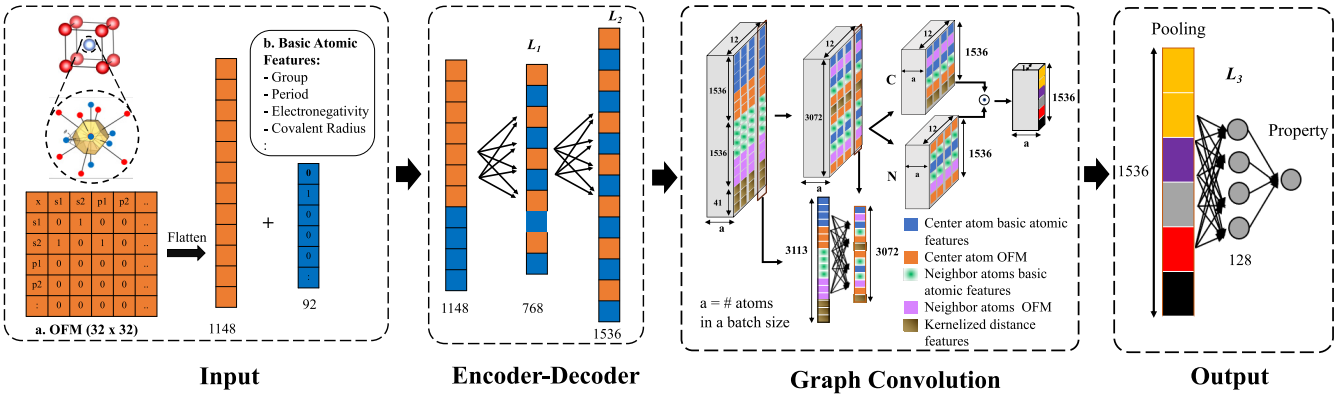

FIG. 2. The structure of the OGCNN framework. It can be divided into four modules, the input, encoder-decoder, graph convolution, and output modules.

neighbor atoms, denoted as n. The 14 neighbor atoms include eight nearest Ti atoms and six next-nearest Fe atoms. Figure 1 shows the formation of a Voronoi polyhydron between the center Fe atom and its 14 neighbor atoms which has the shape of a truncated octahedron. The OFM consists of two parts: (1) a weight function w_{cn} associated with the center Fe atom and any of these 14 neighbor atoms (center-neighbor pair). w_{cn} is calculated by multiplying θ_{cn}, the solid angle subtended at the center atom by the face of the Voronoi cell corresponding to the neighbor atom, i.e., the solid angle between center-neighbor pairs in the Voronoi cell, with $\zeta(r_{cn})$ which is a function of the distance between them $[w_{cn}(r_{cn}) = \theta_{cn} \times \zeta(r_{cn})]$. $\zeta(r_{cn})$ incorporates the information on the size of valence orbitals of the center-neighbor pairs as well as their interactions. (2) A 1D binary vector representation of each atom. The electron configuration of valence orbitals for each atom is encoded into a 1D binary 32×1 vector (Fig. 1). To construct the OFM for the center Fe atom, we sum the matrix product for each center-neighbor pair and multiply it with the corresponding weight function. This results in a 32×32 matrix. Finally, to incorporate the information of the center Fe atom, we concatenate its 1D binary vector to the 32×32 matrix, resulting in a 32×33 OFM for the center Fe atom,

$$X^c = \overrightarrow{O}^{cT} + \sum_{n=1}^{M} \overrightarrow{O}^{cT} \overrightarrow{O}^{n} \theta_{cn} \zeta(r_{cn}). \tag{1}$$

Equation (1) describes the mathematical formulation of the OFM. X^c is the OFM for the center Fe atom, M is the number of neighbor atoms surrounding the center Fe atom, $\overrightarrow{O}^c$ and $\overrightarrow{O}^n$ are the 1D binary vectors for the center Fe and its 14 neighbor atoms, respectively, and $\overrightarrow{O}^{cT}$ is the transpose of $\overrightarrow{O}^c$. The incorporation of geometry as weight enables to encode the local chemical environments through orbital-orbital interactions. To investigate the efficiency of our network, we examined different $\zeta(r_{cn})$ functions including $\frac{1}{r_{cn}}$, $\frac{1}{r_{cn}^2}$, $\frac{1}{r_{cn}^4}$ and $\frac{1}{r_{cn}^6} - \frac{1}{r_{cn}^{12}}$. Subsequently, the $\zeta(r_{cn})$ function that resulted in best performance was selected. We note that, in Voronoi polyhedra, large solid angles correspond to a shorter distance between two adjacent atoms and vice versa. In addition, such Voronoi polyhedra between the center and the neighbor atoms capture the geometry of the local environments of atoms. If only the distances between the center and the neighbor atoms are considered, the geometry will not be captured correctly.

Once we convert the orbital-orbital interactions between each atom and its neighbors into the OFM representation, we use the GCNN and couple it with the OFM. We call this new model the OGCNN. The OGCNN network can be considered as a combination of four modules (Fig. 2). The first module, input module, takes the basic atomic and OFM features. In this module, the embeddings for all crystals in a batch are generated. The basic atomic features include properties, such as the group number, the period number, and electronegativity. The list of 92 basic atomic features are provided in the Supplemental Material [36]. To include the OFM features in the input module, the 32×33 OFM features corresponding to each atom are flattened into a 1056×1 vector. The atom features are constructed by combining the 92×1 basic atomic features and 1056 OFM features forming a 1148×1 vector for each atom in the crystal generating a unique representation for all crystals [Eq. (2)],

$$v_i = [v_{oi}] + [v_{ai}], \tag{2}$$

where v_{oi} and v_{ai} are the OFM and basic atomic features, respectively. The second module, the encoder-decoder module learns important features among atom features by employing a multilayer perceptron (MLP) with two fully connected layers. The MLP acts as an encoder-decoder network which comprises 1148 neurons at the encoder input, 768 neurons in the hidden layer, and 1536 neurons at the decoder output. Using such an architecture enables the network to select the most significant features among the pool of basic atomic and OFM features (Fig. 2).

In this paper, we consider the crystal structure as a graph [34]. A crystal graph is an undirected graph in which the atoms are considered as nodes and the bonds as the edges, and each node has a combination of basic atomic and OFM features [Eq. (2)]. This atom features vector is then transformed as explained in the encoder-decoder module to generate V_i that includes the most important and relevant features. An important aspect of the crystal graph is that different atoms can be connected with more than one bond indicating multiple edges among the nodes of the graph. To incorporate the influence of neighbor atoms, the kernelized distance features between the ith and the jth atoms are captured by the vector

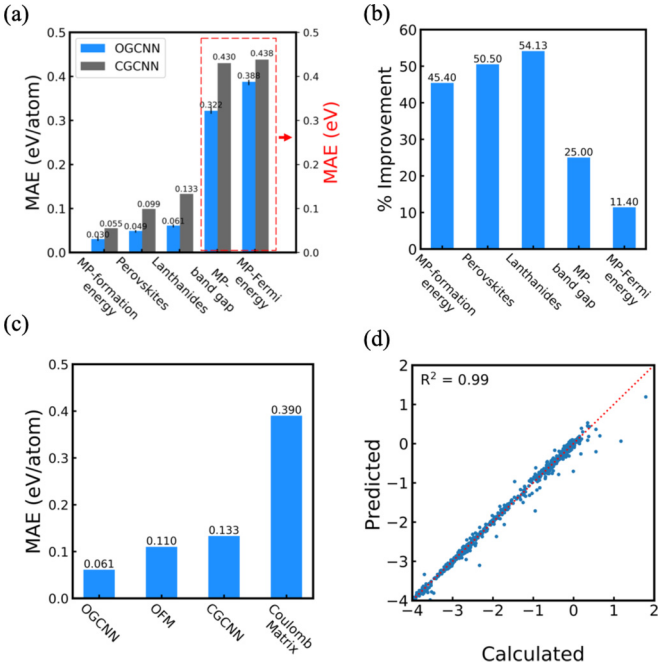

FIG. 3. The test set performance of the OGCNN in different properties predictions across classes of material. (a) Comparison between MAE values of the OGCNN and the CGCNN on test sets for five different datasets. (b) Percentage reduction of the MAE values in (a) when the OGCNN method is used for training over the CGCNN method. A similar train-validation-test ratio was chosen for the OGCNN and CGCNN networks. (c) The MAE values for the prediction of formation energies of the lanthanides dataset using different crystal representations. (d) Comparison of predicted formation energies of 741 test entries of lanthanides using the OGCNN against the DFT-calculated values.

$u_{(i,j)_k}$ where k indicates the kth bond between them. The convolution operation is then performed as in Ref. [34],

$$V_i^{(t+1)} = V_i^{(t)} + \sum \sigma\left(z_{(i,j)_k}^{(t)} W_f^{(t)} + b_f^{(t)}\right) \odot g\left(z_{(i,j)_k}^{(t)} W_s^{(t)} + b_s^{(t)}\right), \tag{3}$$

where $z_{(i,j)} = V_i \oplus V_j \oplus u_{(i,j)_k}$, σ is a sigmoid activation function and g is the softplus function [37]. W and b indicate the weights and bias in the network, respectively.

The convolution operation is performed three times in the OGCNN network. Subsequently, a summation operation is performed over all the neighbors to aggregate the contribution of neighbor atoms which is then sent to the output module. Finally, in the output module, a pooling operation is performed on the output from the graph convolution module to map the properties to a crystal level. The output of the pooling layer is, subsequently, used to predict the target property via a fully connected network with two layers. More details about the architecture of the OGCNN model and different hyperparameters optimized for training the network are available in the Supplemental Material [36].

III. TRAINING AND RESULTS

To train the OGCNN model, we used five different DFT-calculated datasets that include a diverse set of inorganic crystals ranging from metals to complex minerals and oxides [4,38] . The details about these datasets are provided in the Supplemental Material [36]. To examine the generality of the model for predicting a wide variety of properties, we trained the OGCNN model for different properties including formation energy, band gap, and Fermi energy. For training the OGCNN model, we used mean-square loss as a loss function and stochastic gradient descent as an optimizer. Additionally, for all cases, the entire datasets were split into 80,10, and 10% for training, testing, and validation, respectively. Moreover, to avoid any bias during the training process, a five fold cross validation is used to split the datasets, and only their average values are reported [39]. It must be noted that the OGCNN model was trained for 100 epochs and the weights of the model where lowest validation error was observed were used to predict the properties of crystals in the test set. The results for the OGCNN and other models on the test sets are summarized in Fig. 3 and Table I. Figure 3(a) shows that, for all properties and datasets, the MAE values when using the OGCNN are significantly lower compared to that of the CGCNN. Figure 3(b) shows the percentage improvement for prediction accuracy using the OGCNN over the CGCNN. The highest improvement in performance was achieved for the lanthanides dataset: the OGCNN yields a MAE value of 0.061 eV/atom, whereas the CGCNN yields a MAE value of 0.133 eV/atom. This corresponds to 54% improvement in the accuracy prediction for the OGCNN over the CGCNN. On the other hand, the lowest performance over the CGCNN was achieved for the prediction of the Fermi energies of crystals from the Materials Project (MP)-Fermi energy that is 0.38 eV corresponding to an improvement of 11% over the CGCNN. Similarly, for other properties and datasets including formation energies of perovskites, formation energies of crystals from MP-formation

TABLE I. The mean absolute error values for test sets of five different datasets with the OGCNN and the CGCNN have been compared with the ones using the SOAP and the MBTR material representations.

	Material representations				
Dataset	OGCNN	CGCNN	SOAP	MBTR	Unit
Lanthanides-formation energy	0.06	0.13	0.09	0.28	eV/atom
Perovskites-formation energy	0.05	0.09	0.11	0.09	eV/atom
MP-formation energy	0.03	0.05	0.05	20	eV/atom
MP-band gap	0.32	0.43	0.33	0.69	eV
MP-Fermi energy	0.38	0.43	0.38	0.82	eV

energy, and band gaps of crystals from MP-band gap, a reduction of 50%, 45%, and 25%, respectively, in the MAE values were obtained using the OGCNN over that of the CGCNN. To further benchmark the OGCNN, we compared the performance of the OGCNN in training the lanthanides dataset with some other material representations. For the lanthanides dataset, using the OFM and the Coulomb matrix representations and by using kernel ridge regression, the MAE values of 0.11 and 0.30 eV/atom have been reported [22,26]. The CM representation has the lowest performance with a MAE of 0.39 eV/atom followed by the CGCNN, the OFM, and the OGCNN with MAE values of 0.13, 0.11, and 0.06 eV/atom, respectively [Fig. 3(c)]. The predicted formation energies of 741 test entries in lanthanides dataset using the OGCNN against the DFT-calculated values is also shown in Fig. 3(d). We also benchmarked our results against two previously developed state-of-the-art descriptors for encoding atomic structures including the MBTR and SOAP [17,20,40]. Further details about the MBTR and SOAP hyperparameters optimization can be found in the Supplemental Material [36]. In Table I, the performance of the OGCNN with the CGCNN, SOAP, and MBTR descriptors when used to predict different properties corresponding to five datasets were compared. We found that OGCNN exhibits highest performance among all. The only exception is the Fermi energy property where both the OGCNN and the SOAP performed equally well. We would like to emphasize that the MAE values for some properties in this paper are within a narrow range from the DFT-calculated values (Table S4 in the Supplemental Material [36]). For instance, the formation energy predictions using the OGCNN model for different datasets are within a range of 0.03–0.06 eV/atom from the DFT-calculated values. The MAE value for the DFT calculations for formation energy with respect to experimental measurements is within the range of 0.081–0.136 eV/atom. Moreover, the desired chemical accuracy for the formation energy is on the order of 0.04 eV/atom [38,41]. Similarly, for the band-gap property, a MAE value of the 0.6 eV for the DFT calculations has been reported, and using OGCNN, we obtained a MAE value of 0.32 eV [42]. Therefore, given the relatively low error in the predicted properties using the OGCNN, it can be reliably used to predict properties of new materials.

IV. CONCLUSION

In this paper, we proposed the OGCNN, which embeds atomic orbital-orbital interactions features and basic atomic features. The OGCNN, then, was applied to different datasets to predict a wide range of material properties of versatile structures. The prediction accuracy of the OGCNN model is significantly higher than that of previously reported models. The inclusion of orbital-orbital interactions to encode the local chemical environments, and using the encoder-decoder network were the fundamental reasons behind superior performance of the OGCNN. We expect this model to be applicable to a broader range of material discovery applications.

The Github Repository for the OGCNN can be found at Ref. [43].

[1] A. G. Franceschetti and A. Zunger, Nature (London) **402**, 60 (1999).

[2] G. Ceder, Y.-M. Chiang, D. R. Sadoway, M. K. Aydinol, Y.-I. Jang, and B. Huang, Nature (London) **392**, 694 (1998).

[3] G. H. Jóhannesson, T. Bligaard, A. V. Ruban, H. L. Skriver, K. W. Jacobsen, and J. K. Nørskov, Phys. Rev. Lett. **88**, 255506 (2002).

[4] I. E. Castelli, D. D. Landis, K. S. Thygesen, S. Dahl, I. Chorkendorff, T. F. Jaramillo, and K. W. Jacobsen, Energy Environ. Sci. **5**, 9034 (2012).

[5] P. Hohenberg and W. Kohn, Phys. Rev. **136**, B864 (1964).

[6] L. M. Ghiringhelli, J. Vybiral, S. V. Levchenko, C. Draxl, and M. Scheffler, Phys. Rev. Lett. **114**, 105503 (2015).

[7] A. Seko, A. Togo, H. Hayashi, K. Tsuda, L. Chaput, and I. Tanaka, Phys. Rev. Lett. **115**, 205901 (2015).

[8] A. M. Deml, R. O'Hayre, C. Wolverton, and V. Stevanović, Phys. Rev. B **93**, 085142 (2016).

[9] B. Meredig, A. Agrawal, S. Kirklin, J. E. Saal, J. W. Doak, A. Thompson, K. Zhang, A. Choudhary, and C. Wolverton, Phys. Rev. B **89**, 094104 (2014).

[10] P. Dey, J. Bible, S. Datta, S. Broderick, J. Jasinski, M. Sunkara, M. Menon, and K. Rajan, Comput. Mater. Sci. **83**, 185 (2014).

[11] D. Xue, P. V. Balachandran, J. Hogden, J. Theiler, D. Xue, and T. Lookman, Nat. Commun. **7**, 11241 (2016).

[12] O. Isayev, C. Oses, C. Toher, E. Gossett, S. Curtarolo, and A. Tropsha, Nat. Commun. **8**, 15679 (2017).

[13] Q. Zhou, P. Tang, S. Liu, J. Pan, Q. Yan, and S.-C. Zhang, Proc. Natl. Acad. Sci. USA **115**, E6411 (2018).

[14] X. Ma, Z. Li, L. E. K. Achenie, and H. Xin, J. Phys. Chem. Lett. **6**, 3528 (2015).

[15] J. Schmidt, J. Shi, P. Borlido, L. Chen, S. Botti, and M. A. L. Marques, Chem. Mater. **29**, 5090 (2017).

[16] Y. Liu, T. Zhao, W. Ju, and S. Shi, J. Materiomics **3**, 159 (2017).

[17] A. P. Bartók, R. Kondor, and G. Csányi, Phys. Rev. B **87**, 184115 (2013).

[18] J. Behler and M. Parrinello, Phys. Rev. Lett. **98**, 146401 (2007).

[19] J. Behler, J. Chem. Phys. **134**, 074106 (2011).

[20] H. Huo and M. Rupp, Unified representation of molecules and crystals for machine learning, arXiv:1704.06439 (2017).

[21] O. Isayev, D. Fourches, E. N. Muratov, C. Oses, K. Rasch, A. Tropsha, and S. Curtarolo, Chem. Mater. **27**, 735 (2015).

[22] M. Rupp, A. Tkatchenko, K.-R. Müller, and O. A. von Lilienfeld, Phys. Rev. Lett. **108**, 058301 (2012).

[23] L. Ward, A. Agrawal, A. Choudhary, and C. Wolverton, npj Comput. Mater. **2**, 16028 (2016).

[24] W. Ye, C. Chen, Z. Wang, I.-H. Chu, and S. P. Ong, Nat. Commun. **9**, 3800 (2018).

[25] K. T. Schütt, H. Glawe, F. Brockherde, A. Sanna, K. R. Müller, and E. K. U. Gross, Phys. Rev. B **89**, 205118 (2014).

[26] T. L. Pham, H. Kino, K. Terakura, T. Miyake, K. Tsuda, I. Takigawa, and H. C. Dam, Sci. Technol. Adv. Mater. **18**, 756 (2017).

[27] J. Gomes, B. Ramsundar, E. N. Feinberg, and V. S. Pande, arXiv:1703.10603.

[28] S. Back, J. Yoon, N. Tian, W. Zhong, K. Tran, and Z. W. Ulissi, J. Phys. Chem. Lett. **10**, 4401 (2019).

[29] A. Palizhati, W. Zhong, K. Tran, S. Back, and Z. W. Ulissi, J. Chem. Inf. Model. **59**, 4742 (2019).

[30] Z. Wu, B. Ramsundar, E. Feinberg, J. Gomes, C. Geniesse, A. S. Pappu, K. Leswing, and V. Pande, Chem. Sci. **9**, 513 (2018).

[31] Z. Li, X. Ma, and H. Xin, Catal. Today **280**, 232 (2017).

[32] D. Duvenaud, D. Maclaurin, J. Aguilera-Iparraguirre, R. Gómez-Bombarelli, T. Hirzel, A. Aspuru-Guzik, and R. P. Adams, in *Proceedings of the 28th International Conference on Neural Information Processing Systems, NIPS'15* (MIT Press, Cambridge, MA, 2015), Vol. 2, pp. 2224–2232.

[33] Z. Cao, Y. Dan, Z. Xiong, C. Niu, X. Li, S. Qian, and J. Hu, Crystals **9**, 191 (2019).

[34] T. Xie and J. C. Grossman, Phys. Rev. Lett. **120**, 145301 (2018).

[35] T.-L. Pham, N.-D. Nguyen, V.-D. Nguyen, H. Kino, T. Miyake, and H.-C. Dam, J. Chem. Phys. **148**, 204106 (2018).

[36] See Supplemental Material at https://link.aps.org/supplemental/10.1103/PhysRevMaterials.4.093801 for further details about model architecture, training, and hyperparameters optimization.

[37] X. Glorot, A. Bordes, and Y. Bengio, in *Proceedings of the Fourteenth International Conference on Artificial Intelligence and Statistics*, Proceedings of Machine Learning Research edited by G. Gordon, D. Dunson, and M. Dudík (PMLR, Fort Lauderdale, FL, 2011), Vol. 15, pp. 315–323.

[38] A. Jain, S. P. Ong, G. Hautier, W. Chen, W. D. Richards, S. Dacek, S. Cholia, D. Gunter, D. Skinner, G. Ceder, and K. A. Persson, APL Mater. **1**, 011002 (2013).

[39] P. Refaeilzadeh, L. Tang, and H. Liu, *Encyclopedia of Database Systems*, edited by L. LIU and M. T. ÖZSU (Springer, Boston, MA, 2009), pp. 532–538.

[40] L. Himanen, M. O. Jäger, E. V. Morooka, F. F. Canova, Y. S. Ranawat, D. Z. Gao, P. Rinke, and A. S. Foster, Comput. Phys. Commun. **247**, 106949 (2020).

[41] S. P. Ong, W. D. Richards, A. Jain, G. Hautier, M. Kocher, S. Cholia, D. Gunter, V. L. Chevrier, K. A. Persson, and G. Ceder, Comput. Mater. Sci. **68**, 314 (2013).

[42] S. Kirklin, J. E. Saal, B. Meredig, A. Thompson, J. W. Doak, M. Aykol, S. Rühl, and C. Wolverton, npj Comput. Mater. **1**, 15010 (2015).

[43] Github repository for the OGCNN, https://github.com/RishikeshMagar/OGCNN.